Corrosion, Passivation, and the Effect of Water Addition on an n-GaAs(100)/Methanol Photoelectrochemical Cell

T. A. Abshere and G. L. Richmond*

Department of Chemistry and Materials Science Institute, University of Oregon, Eugene, Oregon 97403

Received: October 25, 1999; In Final Form: December 23, 1999

A combination of picosecond photoluminescence and electrochemical studies reveals information about the GaAs/methanol interface. The electrochemistry occurring at the solid/nonaqueous liquid junction is found to have a strong influence on the observed photoluminescence as seen by photoluminescence vs voltage (PL−*V*) scans and by trends in the time-resolved photoluminescence decays. The effect of corrosion of the cell on the PL−*V* profile is examined in detail. It is found that the inclusion of the redox couple gives some protection from corrosion, but the addition of a small amount of water to the nonaqueous cell gives even more. Further water additions lead the cell back to a state that is conducive to corrosion and eventually leads to Fermi level pinning of the GaAs.

I. Introduction

The potential applications of n-GaAs in photoelectrochemical cells (PEC) have long been hampered by the anodic corrosion of GaAs in aqueous solutions. Much work has been done to try to understand the process of corrosion of a PEC[1−12] and to understand other interfacial phenomena such as passivation,[4,13−21] charge transfer,[22−25] photowashing,[26−29] and Fermi level pinning.[14,30−33] GaAs is an exceptional material for the study of these types of phenomena since it both photoluminesces and is capable of photoelectrochemical energy conversion. Relatively simple photocells can be made with GaAs in either aqueous or nonaqueous environments with a variety of redox couples and the possibility of adding passivating overlayers. In this work, picosecond induced photoluminescence and photocurrent measurements will be used to gain a better understanding of the interfacial characteristics of an n-GaAs(100)/methanol PEC.

In a previous publication, we showed that even trace amounts of water in a (seemingly) anhydrous n-GaAs/methanol PEC is enough to cause the cell to photocorrode when the cell potential is held in the deep depletion regime.[34] The current work is a continuation of the investigation of the interfacial characteristics of the n-GaAs/methanol junction in a PEC. The strong influence that the electrochemistry occurring in the cell has on the picosecond photoinduced luminescence will be explored in detail. Also, the photoluminescence (PL) and electrochemistry of these cells will be examined under a variety of conditions to gain information about corrosion, photowashing, charge transfer, and other interfacial processes.

The studies described herein involve four types of experiments. PL−*V* curves are examined in detail to study corrosion of the GaAs and to show the strong influence of the electrochemistry occurring at the interface on the measured PL. PL−*V* curves have been used extensively in this lab to study both aqueous[3,35,36] and nonaqueous[34] GaAs PEC's. Comparisons of the PL−*V* curves are made with the PL−*V* behavior predicted by the modified dead layer model (MDLM).[37,38] Time-resolved photoluminescence (TRPL) decays are measured at a variety of potentials to show changes in the decay rate with potential. Current vs applied potential (*I*−*V*) measurements give complementary information to the photoluminescence measurements. They are useful for determining which changes in the cell affect charge transfer rates and/or chemistry occurring at the interface. Finally, PL vs time (PL−*T*) measurements have been made to examine the changes in PL with light exposure at individual applied potentials. Details about the scan rates, laser powers, repetition rates, and applied potentials can be found in the figure captions for individual experiments. General cell configuration and contents information is found in section II.

One of the more interesting results included in this paper is the observation of a dip in the PL−*V* profile (in a cell containing the redox couple) in a narrow potential range within the depletion regime. The decrease in PL is attributed to majority carrier electrochemical effects. Reduction current from the majority carrier causes a deviation in the PL−*V* behavior from that predicted by the MDLM. *I*−*V* curves and TRPL decay measurements are used in combination with the PL−*V* data to support this assertion. Other parts of the studies described herein examine the photocorrosion of the GaAs surface and the cell parameters that affect the rate of the photocorrosion. The changes in PL−*V* curves that are indicative of corrosion are reviewed so that comparisons can be made among a variety of PL−*V* curves that reflect changes in individual cell parameters. Varying the total time under illumination, the presence of redox couple, and the water content of the cell all result in changes in the PL−*V* behavior of the cell that can be correlated with surface reactivity and corrosion. The implications of the various observed PL−*V* behaviors to the physical and chemical properties of the n-GaAs electrochemical cell are discussed.

II. Experimental Considerations

The experiments were performed on n-GaAs (100) crystal wafers (Crystal Specialties) with a (Si doped) carrier concentration of $(2-4) \times 10^{17}$ cm^{-3}. The back of the n-GaAs was etched for 2 min with a solution of 2:1:1 H_2SO_4 (96.7%):H_2O:H_2O_2 (30%) and then placed in contact with a copper electrode using an indium/gallium eutectic. The front surface of the n-GaAs was etched (0.05% Br_2/MeOH solution for 15 s followed by 1 M KOH for 30 s, and repeated at least three times) before introducing the sample into a drybox where the rest of the

10.1021/jp993782v CCC: $19.00 © 2000 American Chemical Society
Published on Web 01/27/2000

electrochemical cell and the dried chemicals were held. The cells were put together inside the drybox, which generally contained <0.2 ppm of O_2, and sealed before being brought out and placed in front of the laser. All chemicals other than ferricenium and $LiClO_4$ were obtained from Aldrich. Anhydrous methanol (<0.002% H_2O) was purified by distilling over sodium followed by three freeze−pump−thaws to degass before introduction to the drybox. $LiClO_4$ was obtained from Alfa Aesar and dried by heating under vacuum for several days. Ferrocene was used as received. Ferricenium was oxidized electrochemically from ferrocene in the presence of $LiClO_4$ to give the ferricenium perchlorate salt, which was dried under vacuum. Unless specifically noted in the paper, the nonaqueous cells contained 0.7 M $LiClO_4$:0.02 M $FeCp_2$:0.005 M $FeCp_2$ + ClO_4^- in 50 mL of methanol.

For all experiments, the cells were held under potentiostatic control in a three-electrode configuration. The counter electrode (CE) was a platinum wire. The reference electrode (RE) was either a platinum wire poised at the electrolyte equilibrium potential or a Ag/(0.01 M)$AgNO_3$ nonaqueous reference (from BAS) in a 0.7 M $LiClO_4$ methanol solution separated from the main cell by a vicore frit. The Ag/$AgNO_3$ electrode potential was measured to be 0.46 V vs a saturated calomel electrode. The equilibrium cell potential (Pt. vs Ag/$AgNO_3$) was measured to be −0.31 V. All potentials in the paper are scaled to the Ag/$AgNO_3$ reference electrode for clarity. The working electrode typically had a dark open circuit voltage (V_{oc}) of −0.42 V vs Ag/$AgNO_3$ immediately after introduction to the cell. According to work by Ba et al.,[33] the flat band potential (V_{fb}) for the n-GaAs/methanol cell is −1.5 V vs Ag/$AgNO_3$. V_{fb} was verified by Mott−Schottky analysis. The working electrode was placed within 1 cm of the optical window to minimize any absorption effects of the electrolyte on either the laser light or the band gap luminescence. None of the solutions were stirred during the experiments reported in this paper.

All of the experiments in this paper were performed either without any applied potential or within the potential range from flat band potential (V_{fb} = −1.5 V) to deep depletion. When no potential is applied, the cell is at the open circuit potential (Voc) which varies depending on illumination. All investigated potentials more positive (less negative) than V_{fb} are in the depletion regime where a space charge layer exists in the semiconductor near the interface.

For the photoluminescence studies, the n-GaAs is illuminated at near normal incidence by the pulse compressed (≈5 ps) frequency doubled (to 532 nm) output of a mode-locked Nd:YAG laser. Details of the laser system have been described elsewhere.[36,39] Selecting pulses with an acoustooptic modulator (AOM) controls the repetition rate with an extinction coefficient in excess of 200:1. Power is adjusted with a half-wave plate/polarizer. Band gap luminescence (855 nm) is filtered with a 610 nm long-pass filter and monochromator before being collected by a cooled microchannel plate photomultiplier tube feeding a 1.8 GHz amplifier attached to a constant fraction discriminator. The TRPL decays are taken with a time-correlated single photon counting technique[40] using the discriminator as a start pulse and a fast photodiode, detecting a portion of the pulse separated prior to illuminating the sample, as the stop pulse. The microchannel plate has a time resolution of 11.1 ps; however, system response functions (obtained by measuring scattered 532 nm light) have a full width/half-maximum (fwhm) of approximately 80 ps. For qualitative comparisons, the decays are viewed as measured without deconvolving the system response function.

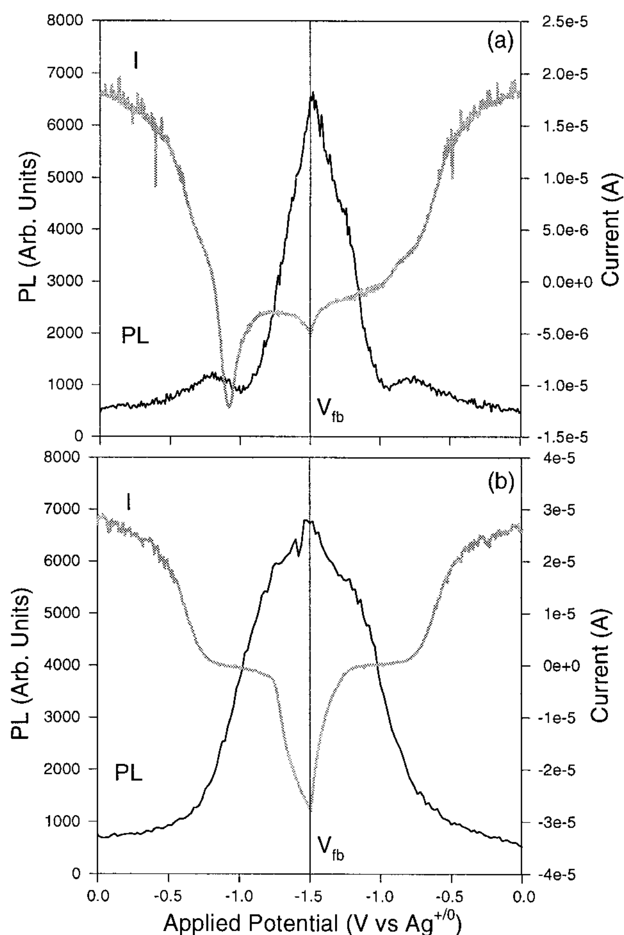

Figure 1. Photoluminescence and current as a function of applied potential in n-GaAs/methanol cells with (a) the ferrocene/ferricenium redox couple and (b) no included redox couple. Both scans were measured with a 10 mV/s scan rate and were illuminated with a photon flux of 1.6 × 10^{13} photons/(cm^2·pulse) at 951 kHz repetition rate.

The spot size illuminating the n-GaAs was characterized by knife-edge measurements independently across the vertical (ω_v) and horizontal (ω_h) transverse profiles of the beam. The beam is elliptical at the sample, most likely a result of the use of the AOM for eliminating pulses earlier in the beam path. Assuming an approximately Gaussian transverse spatial profile, the distance between knife-edge positions passing 16% and 84% of the total beam energy was used to approximate the Gaussian beam radius ω, which is the half-width at $1/e$ of maximum for field amplitude, or $1/e^2$ of maximum for intensity.[41] The Gaussian beam radius ω is related to the fwhm for the intensity by fwhm = $(2 \ln 2)^{1/2}\omega$. The area of the spot used for measuring photon flux (photons/cm^2·pulse) was taken to be $\pi\omega_v\omega_h = 1.70 \times 10^{-4}$ cm^2, where ω_v = 60 μm and ω_h = 90 μm.

III. Results and Discussion

IIIA. Effects of Electrochemistry on PL−*V* Behavior. Figure 1 shows the photoluminescence and the current of two cells as the voltage is swept from 0.0 to −1.5 V and back to 0.0 V at a scan rate of 10 mV/s. One cell contains the ferrocene/ferricenium redox couple (Figure 1a) and the other cell has no redox couple (Figure 1b). It is clear from Figure 1a that when the redox couple is included, there is a significant hysteresis in both the current and the photoluminescence as the potential is cycled between the two limits stated above. This is particularly apparent for the $I-V$ curve, which is typical of an unstirred PEC containing a reversible redox salt.[9,42,43] The PL−V curve,

however, is quite atypical as compared to other semiconductor systems found in the literature.[38,44−47] The two primary characteristics of the PL−V curve that differ from other systems will be described and possible causes of these differences will be discussed.

The dead layer model (DLM) can, as a first approximation, predict the voltage dependence of the photoluminescence for many semiconductor/metal[44,47] and semiconductor/electrolyte[37,38,45,46] junctions. The model has been described in detail elsewhere,[37,38] so only a perfunctory review will be given here. Even though the PL−V of the system currently under investigation deviates from the predictions of the MDLM, it can be used as a guide to the behavior of the carriers and thus is invoked here. In this way, the results of the experiments can be explained in terms of a model prevalent in the literature while at the same time emphasizing the limitations of that model. First, the MDLM will be briefly described. Then the deviations from predicted behavior as seen in Figure 1a will be discussed.

The MDLM predicts the bias dependence of luminescence by assuming a recombination free, or "dead", zone in the semiconductor with the same width (W) as the space charge region (SCR). The primitive version of this model neglects both diffusion from the bulk into the SCR and consumption of holes by either surface recombination or charge transfer across the interface. The luminescence intensity has the form:

$$I_{PL}(W) = I_{max}e^{-\alpha W} \tag{1}$$

where α is the absorption coefficient, I_{max} is the luminescence intensity in the absence of a space charge region, and W is the width of the SCR, which is related to the applied bias $\Delta V = V - V_{fb}$ by

$$W = (2\epsilon\epsilon_o \Delta V/en_d)^{1/2} \tag{2}$$

ϵ_o is the permittivity of free space, ϵ is the dielectric constant, e is the elementary charge, and n_d is the doping density of the semiconductor.

The MDLM takes into account the loss of minority carriers by diffusion and radiationless surface reactions by including the factor $(1 + \alpha L)^{-1}$ into the luminescence intensity. L is the diffution length of the minority carriers. Now the luminescence intensity can be described as

$$I_{PL}(W) = I^{\circ}{}_{PL}e^{-\alpha W} \tag{3}$$

where $I^{\circ}{}_{PL} = (1 + \alpha L)^{-1}I_{max}$. In the MDLM, the functional form of $I_{PL}(W)$ stays the same so only the absolute intensity at V_{fb} differs from the prediction of the primitive DLM.

The PL−V behavior of the PEC under investigation is quite different from that predicted by the MDLM. However, the anomalous characteristics of the PL−V scans can be explained in terms of the breakdown of the assumptions made with the MDLM. Figure 1a shows the potential dependence of the PL and I for the redox couple containing cell as the applied potential (V) is swept at 10 mV/s from 0.0 to −1.5 V (V_{fb}) and back to 0.0 V. The temporal order of the scan follows from left to right, sweeping the potential first toward forward bias and then back toward reverse bias with the turnaround at V_{fb} indicated by the vertical line. The MDLM does not specify the direction the potential is being swept so either half of Figure 1a can be compared with theory.

Figure 1a shows two deviations from MDLM predictions. First, the two halves of the figure are not symmetric. There is more PL present on the right side of the figure than on the left side. Clearly, the direction the potential is swept makes a difference in the PL behavior. Second, there is a dip in the PL with the minimum at approximately −0.65 V. The dip is more prominent on the left side of the figure, which, as stated previously, has less overall PL than the right side.

Our explanation for the observed behavior is as follows. Starting at the left of the graph, at 0.0 V, the semiconductor is in deep depletion. The electrons are strongly driven into the bulk and holes are driven to the surface where they recombine with electrons in a variety of processes. Both the SCR width and the surface recombination velocity (SRV) are at a maximum. The SRV is the nonradiative recombination rate of the minority carriers. The charge separation at this potential quenches much of the PL resulting in the lowest measured PL in the potential region investigated. As the potential is swept toward forward bias, the PL increases as predicted by the MDLM. The band bending is decreased, the SCR is smaller, and there is less positive current (from oxidation of the redox couple), all of which leads to less quenching of the PL. However, from −0.8 to −1.0 V there is a dip in the PL. The band bending and SCR width continue to decrease in this region so the driving force for charge separation is decreasing. According to the MDLM, the PL should increase in this region.

What the MDLM does not include is the forward bias current caused by reduction of the redox couple in solution. The effect of the forward bias current can be seen in the I−V scan taken simultaneously with the PL−V scan in Figure 1a. From the left side of the figure, it can be seen that the dip in PL starts with the beginning of the forward bias current at −0.8 V. The semiconductor bands are bent at this potential so there is a limited concentration of electrons in the conduction band (CB) close to the interface. A portion of those electrons transfer across the interface to reduce the redox couple and are no longer available for radiative recombination. In terms of the MDLM, the additional draw on electrons causes an increase in the width of the dead zone where no radiative recombination occurs, which results in a decrease in the PL. We attribute the dip in PL in Figure 1a to this majority carrier effect.

The cathodic current across the interface results in a decrease in the PL over the entire potential range where the cathodic current flows, but it only results in a visible dip in the PL in a small potential range. After −1.0 V, the band bending is decreased enough for the density of electrons at the interface to overcome the additional draw of the cathodic current and the PL once again begins rising. The PL is still decreased in this region from MDLM predictions but not enough to overcome the increasing PL from the band bending affects. Also, at the same time that the potential is becoming more negative, the magnitude of the cathodic current decreases. From −1.0 V to V_{fb} the PL increases. At V_{fb}, the direction of the scan is reversed. The PL decreases as the semiconductor is swept back into depletion but with a noticeable hysteresis from the left side of the figure. There is more PL on the right side, at least in the region from −1.5 to −0.8 V. This is consistent with the argument above suggesting a decrease in PL from loss of electrons to cathodic current flow. The concentration of the oxidized form of the redox couple near the electrode is not refreshed when the direction of the sweep is switched. The cathodic current is less on the right side of Figure 1a so the loss in PL is also less.

To verify that the effects discussed above resulted from electrochemical processes involving the redox couple, a cell was analyzed containing no redox. The PL−V profile of this cell is shown in Figure 1b. There are two notable features to this scan.

First, the high PL region around V_{fb} is noticeably wider than in the PL−V scan in Figure 1a. A direct comparison between these two scans shows a significant loss in PL in the potential region where the cathodic current flows in the cell containing the redox couple. Second, in Figure 1b there is no dip in PL between −0.8 and −1.0 V. These two features give strong evidence that deviations in the PL−V behavior from the MDLM are from the electrochemistry occurring at the surface of the n-GaAs. The I−V curve taken simultaneously with this scan is also shown in the figure. The positive current in Figure 1b corresponds to corrosion of the cell and the negative current to reduction of the solvent.

This is not the only example of cathodic reactions affecting the PL behavior of an n-GaAs cell. Smandek et al. found hysteresis (including localized dips) in the PL−V behavior of an aqueous n-GaAs PEC in the accumulation potential regime.[38] Here the hysteresis was attributed to reduction processes involving the surface oxide layer of the semiconductor. An important difference with the current work is that the methanol cell under investigation shows a dip in the PL in the depletion regime. A small amount of hysteresis in the PL around the flat band potential has been noted in other systems and attributed to the difficulty in controlling the potential close to flat band.[36] However, that hysteresis did not include any features as significant as the dip seen in Figure 1a, which occurs 600 mV from flat band.

These are the first measurements that we are aware of that show a dip in the PL in the depletion regime of n-GaAs (other than the natural decrease in the PL from band bending predicted by the DLM) in an aqueous or nonaqueous PEC. However, this may simply be due to the absence of PL−V data on PEC's that contain a reversible redox couple with an equilibrium potential within the band gap of GaAs. All of the references above show PL−V scans either for semiconductor/metal Schottky junctions or for semiconductor/electrolyte junctions that have only reverse bias current in the depletion regime. The redox used here ($FeCp_2^{+/0}$) is both reversible and has an equilibrium potential close to the valence band edge of n-GaAs. Since these are desirable qualities for a redox couple in a PEC, studies of PEC's with this configuration are important. It remains to be seen if other redox couples will produce the same PL−V behavior.

There is an alternative interpretation of the PL−V data in Figure 1a that we have discounted. Rather than viewing the anomalous behavior as a dip in the PL at −1.0 V, one might argue that there is instead a peak in the PL at −0.8 V. Looking at the left side of Figure 1a from −0.6 to −1.0 V, there appears to be a small peak corresponding to the region where the photocurrent disappears, rather than a dip where the forward bias current appears. Under this alternative interpretation, the small PL peak would result from a minority carrier effect where the decreasing photocurrent would indicate a decrease in the SRV. This could result in an overall increase in PL as manifested in a small peak.

We do not believe that the alternative interpretation is the best description of the PL−V data for the following reasons. First, in the absence of redox couple (Figure 1b), the range of potentials where the PL is high is much broader than in the cell containing the redox couple (Figure 1a). This suggests that the addition of the redox couple results in an overall reduction in PL intensity near V_{fb}. Second, a comparison of the I−V curve with the PL−V curve in Figure 1a is inconsistent with the alternative interpretation. Under that interpretation, there is an increase in the PL on the left side of Figure 1a because the photocurrent is decreasing in that region. However, on the right side of the figure, in the potential region where the PL is increasing, the photocurrent is also increasing. Viewed in terms of the MDLM, an increasing photocurrent should be quenching the PL, not enhancing it. Under the alternative explanation, there is no consistent correspondence between the photocurrent and the PL behavior so we conclude that this interpretation is incorrect. Interpreting the deviation from MDLM behavior as dips in the PL rather than peaks agrees with the supporting data from the I−V and PL−V scans in Figure 1, a and b, respectively. Therefore, we attribute the anomalous PL−V behavior to a forward bias current effect as described above.

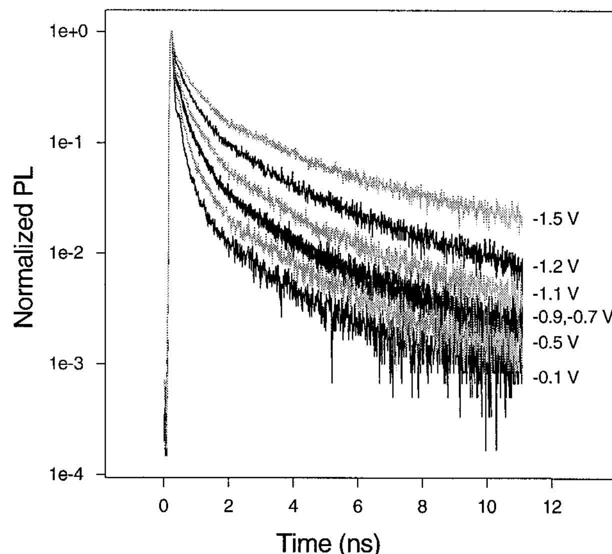

Figure 2. TRPL decays ranging from −1.5 to −0.1 V in an n-GaAs PEC containing the redox couple. The decay rate gets faster as the potential gets closer to −0.1 V except for the two decays at −0.9 and −0.7 V which lie on top of one another. All decays are measured with a photon flux of 1.6×10^{13} photons/(cm^2·pulse) at 951 kHz repetition rate.

IIIB. **TRPL Measurements**. Time-resolved photoluminescence studies can be used to obtain either qualitative or quantitative information about the surface recombination velocity and the rate of PL decay at the semiconductor/liquid interface. In order to determine if the effects leading to the dip in the PL−V scan of Figure 1a affect the measured SRV in these cells, a voltage-dependent TRPL decay study was performed covering the band gap potential range. Figure 2 shows TRPL decays taken at several potentials from V_{fb} to −0.1 V for a cell containing the redox couple. The trend in the decays matches the trend in the PL−V scan on the right side of Figure 1a. The decay at V_{fb} has the slowest decay rate, which corresponds to the lowest measured SRV. Values for the SRV can be determined by modeling the TRPL decays[4,37,39] but that is not necessary for the qualitative discussion here. With increased reverse bias, the applied potential moves the semiconductor into the depletion regime, so the decay rate and SRV increase. Similar to the PL−V scan in Figure 1a, there is an anomaly to this trend. The decays measured at −0.9 and −0.7 V have the same decay rate and measured SRV. The decays taken at potentials more positive than −0.7 V returned to the earlier trend with each successive decay having faster decay rates and larger measured SRV's. The static SRV from −0.9 to −0.7 V (which may be looked at as a relative decrease in the SRV at −0.7 V compared with the trend) occurs in the potential region corresponding to the recovery of the PL after the forward bias current goes to zero. If this interpretation is correct, then the TRPL decay data suggests that the forward

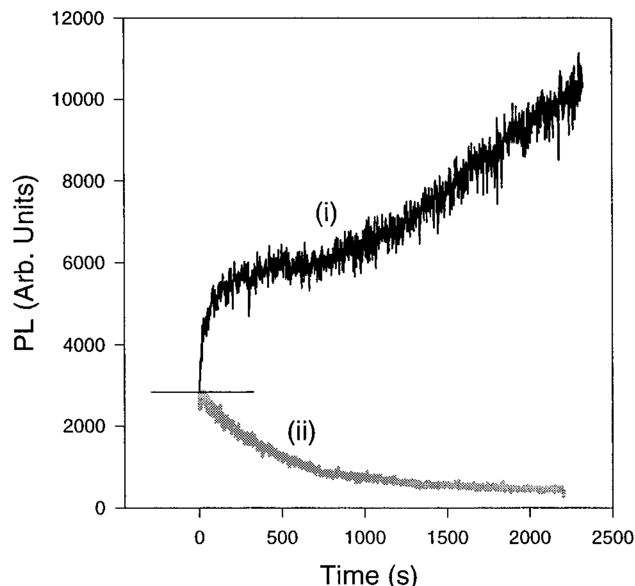

Figure 3. Photoluminescence over time at (i) −1.50 V showing the effects of photowashing and at (ii) 0.0 V showing photocorrosion of the standard GaAs cell containing the redox couple. Both scans were measured while the cell was illuminated with a photon flux of 1.6 × 10^{13} photons/(cm^2•pulse) at 951 kHz repetition rate.

bias current (between −0.7 and −0.9 V of Figure 1a) not only decreases the overall PL but also causes faster decay rates and a higher measured SRV.

IIIC. **PL−*T* Measurements**. Figure 3 shows the PL measured while the potential is held over a long period of time at either (i) V_{fb} or (ii) 0.0 V. Monitoring the PL over time at a specific potential gives a qualitative account of the stability of the GaAs surface at that potential. These scans show the sensitivity of the condition of the interface to the applied potential. Unlike the TRPL decays measured at V_{fb}, no preliminary sweeps were made of the potential before the PL−*T* measurements were started. When the cell is held at V_{fb}, the PL increases over time. This is a result of photowashing of the GaAs. The light exposure causes a reduction of the density of surface states (SS), which results in an overall increase in PL. When the cell is held at 0.0 V, the PL decreases over time. This is from photocorrosion of the cell, where the density of SS increases over time. At intermediate potentials the interface is stable and there is no change in PL over time (not shown in figure). These effects have been investigated previously[34] for this system using TRPL decays. The PL−*T* scans provide additional support of the previous data and provide a framework of the competing effects occurring in different potential ranges in these cells.

IIID. **Effects of Photocorrosion**. Several of the cell parameters have been investigated to determine how they qualitatively affect the rate of corrosion of the cell. PL−*V* scans are useful for this type of investigation because the loss in PL with corrosion can be followed over several full sweeps of the potential. The effect of light exposure over time is inherently seen by comparing earlier sweeps with later sweeps within the same PL−*V* scan. In previous corrosion studies, PL−*V* scans have been used to verify that photocorrosion has occurred.[3,35] Figures 4−6 contain PL−*V* scans that have been placed on a PL vs time scale. In all of the scans, the voltage is swept back and forth from 0.0 to −1.5 V several times. Displaying the data in this way allows us to make comparisons between individual sweeps within the same scan as well as comparing one scan to another. Figure 4 shows the changes in the PL−*V* profile as a

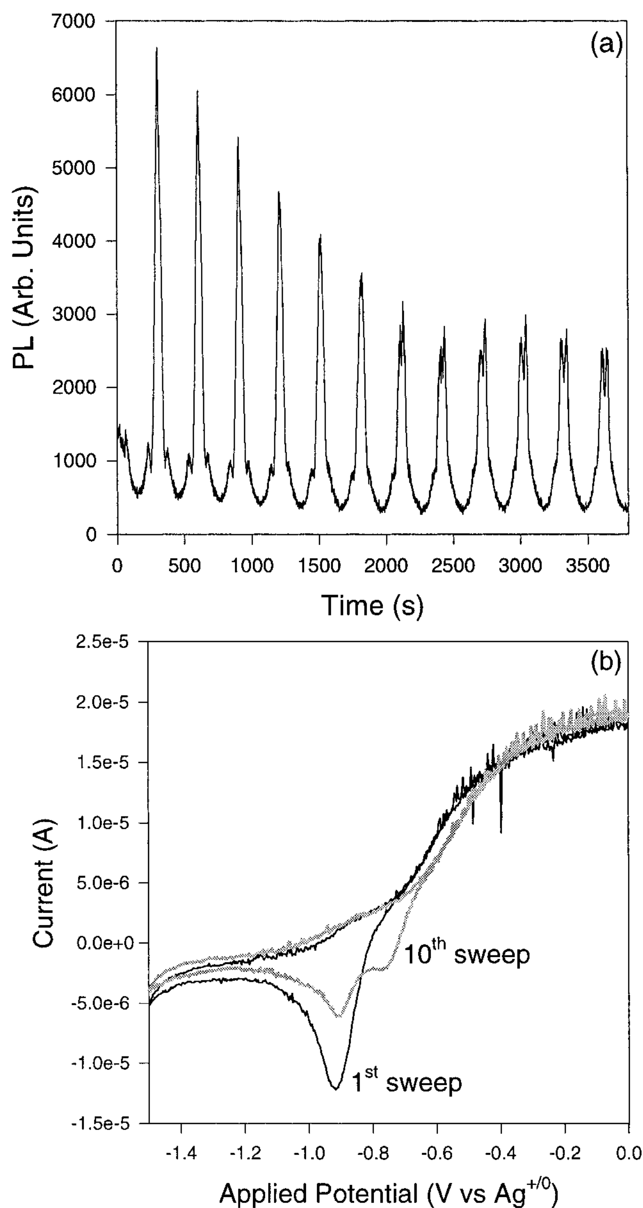

Figure 4. (a) PL over time as the voltage is swept back and forth from −1.50 to 0.0 V at 10 mV/s, corroding the n-GaAs PEC containing the redox couple. (b) Concurrent *I*−*V* curves for the first and 10th full sweeps shown in (a). Both scans were measured while the cell was illuminated with a photon flux of 1.6 × 10^{13} photons/(cm^2•pulse) at 951 kHz repetition rate.

cell corrodes. The remaining figures will show the differences in the corrosion of the cell from varying the presence of the redox couple and spiking the cell with water. The latter is discussed in section IIIE.

Figure 4a shows several successive PL−*V* sweeps where the PL is monitored while the voltage is swept at 10 mV/s. The figure shows changes in the PL−*V* profile (of a cell containing the redox couple) which are indicative of corrosion of the cell. First, the PL measured at V_{fb} (PL_{fb}), which is the maximum PL for each sweep, decreases with each successive sweep until it reaches a stable value. In Figure 4a, it took seven full sweeps before the PL_{fb} stabilized. Second, the dip in PL at −1.0 V (described in Figure 1a) disappears as the cell corrodes. The buildup of corrosion induced SS in the band gap decreases the PL on either side of the dip until it blends in and disappears. Finally, the peak at PL_{fb} splits after several sweeps. We are unsure of the cause of this feature but it is likely related to

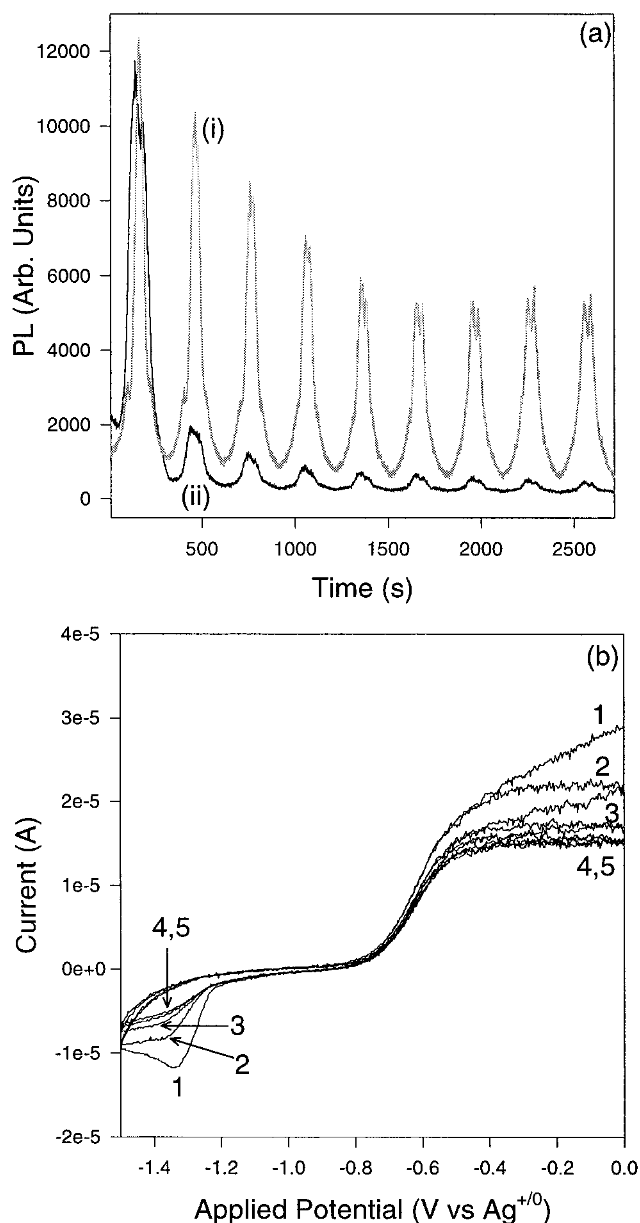

Figure 5. (a) PL over time with voltage sweep as in Figure 4a for cells containing (i) the standard ferrocene/ferricenium redox couple and (ii) no redox couple. (b) $I-V$ curve corresponding to the first five scans of the PL$-V$ scan (a(ii)). Unlike the cells with redox couple, the corrosion of this cell causes a decrease in the photocurrent. All scans were measured while the cell was illuminated with a photon flux of 1.6×10^{13} photons/(cm^2•pulse) at 951 kHz repetition rate.

chemical changes occurring at the n-GaAs surface while reducing the methanol solvent. Cathodic current flow from solvent reduction is visible in the $I-V$ curve shown in Figure 1a at the flat band potential but its effects on the interface are complex and have not been investigated further.

Figure 4b shows $I-V$ curves taken simultaneously with the first full PL$-V$ sweep (black line) and the 10th full PL$-V$ sweep (gray line) from Figure 4a. These $I-V$ curves are typical for fresh (first sweep) and corroded (10th sweep) n-GaAs surfaces, respectively, in a cell containing the redox couple. The portion of the $I-V$ curves corresponding to the sweep into reverse bias (i.e., from -1.5 to 0.0 V) look similar for the two curves. The SS created with photocorrosion of these cells does not affect the photocurrent coming from either oxidation of the redox couple (-1.0 to -0.7 V) or photocorrosion (-0.7 to 0.0 V) of

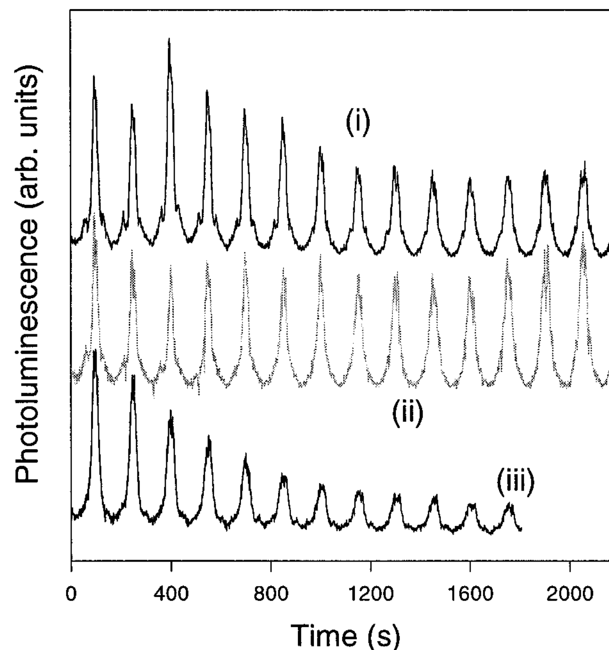

Figure 6. PL over time with the voltage swept between -1.5 and 0.0 V at 20 mV/s for cells (containing the redox couple) with (i) no water added showing corrosion, (ii) 10 μL of water added showing no corrosion, and (iii) 100 μL of water added showing corrosion again. All scans were measured while the cell was illuminated with a photon flux of 1.6×10^{13} photons/(cm^2•pulse) at 951 kHz repetition rate.

the cell. However, the sweep into forward bias (from 0.0 to -1.5 V) looks quite different for the two curves. In the fresh cell, the forward bias sweep shows a current peak at -0.9 V for the reduction of the redox couple and a small current drop near -1.5 V corresponding to the beginning of the solvent reduction peak. In the corroded cell, the reduction current as a whole is smaller but there is additional reduction current around -0.7 V. The buildup of this additional current occurs faster in cells with lower concentrations of redox couple but is entirely absent in the cells tested without any redox couple (not shown in the figure). It appears that the photoinduced SS created by corrosion of the cell do have an impact on the charge transfer across the interface. They do not affect the anodic photocurrent but they do appear to affect the cathodic current. There is complex chemistry occurring at the interface, not just charge transfer to the redox couple. We speculate that the additional cathodic current is associated with reduction either of the oxidized GaAs (from the corrosion process) or of some other corrosion products at the interface.

The inclusion of the redox couple is clearly important to the behavior of the GaAs/methanol interface. To elucidate the passivating effect of the redox couple, PL$-V$ scans of (i) a cell containing the $FeCp_2^{+/0}$ redox couple and (ii) a cell without a redox couple are plotted together in Figure 5a. Both scans were measured at the same scan rate (10 mV/s), at the same laser power, and start at the same potential. Like the PL$-V$ scans shown earlier, the potential is swept from 0.0 to -1.5 V and back. Nine full sweeps are shown for each scan. Since the PL is measured on an arbitrary scale, comparisons are made between scans based on trends and changes occurring within each individual scan. For example, in the scans shown in Figure 5a, the corrosion of the two cells is compared by monitoring changes in the PL_{fb} values within each scan. In scan (i) the PL_{fb} value drops by 16% from the first to the second sweep. The PL_{fb} stabilizes after six sweeps at approximately 50% of the PL_{fb} for the first sweep. In scan (ii) the PL_{fb} drops by 85%

from the first to the second sweep. After six sweeps there is only a small peak visible above the noise. We conclude that the redox couple helps to passivate the n-GaAs surface from corrosion to a limited extent. The corrosion occurs slower and with less quenching of the PL in the cell with redox couple because the redox couple is competing with the corrosion process for the available holes at the interface.

Figure 5b shows the first (5) sweeps of the $I-V$ scan taken simultaneously with the PL$-V$ scan without redox couple in Figure 5a. Since there is no redox couple to oxidize, the photocurrent in this figure is only from corrosion of the cell. Unlike methanol cells that have $FeCp_2$ included,[34] there is a measurable loss in photocurrent as these cells corrode. The corrosion occurring in the absence of redox results in a density of SS, which not only severely inhibits photoluminescence but also inhibits charge transfer across the interface. These results suggest that this corrosion involves the rapid buildup of a much larger density of photoinduced SS than what occurs in the cells with redox couple.

IIIE. **Water Addition**. Water addition to the n-GaAs/methanol cells was investigated previously with $I-V$ curves.[34] The PL$-V$ study presented in Figure 6 confirms the results of the previous study with one significant exception. The $I-V$ study showed the n-GaAs/methanol cells (including the redox couple) have three behavioral regions, depending on the total amount of water added. The PL$-V$ scans in Figure 6 show an additional behavioral region by distinguishing between a fresh cell and a cell with the smallest water addition. The $I-V$ study will be summarized and then the new information from the PL$-V$ study will be discussed.

In both the $I-V$ and the PL$-V$ studies, 18 MΩ Nanopure water was added to a GaAs/methanol PEC containing 50 mL of methanol in 10 μL increments. In the $I-V$ study, the addition of 10$-$40 μL of water appeared to have no effect on the cell. The addition of 60$-$100 μL of water decreased the photocurrent over progressively larger potential regions followed by recovery of the photocurrent when the cell was moved far enough into reverse bias. When 110 μL of water (or more) was added, there was a significant decrease in photocurrent in the entire reverse bias region that was not recoverable. The PL$-V$ study follows this same trend except that there is a difference between the fresh cell and the cell containing 10 to 40 μL of water.

Figure 6 shows PL$-V$ scans taken at 20 mV/s from (i) a freshly prepared cell, (ii) the same cell after 10 μL of water was added by injection, and (iii) the cell after 100 μL of water was added. The fresh cell (containing 50 mL of methanol as the solvent) shows corrosion with a 20 mV/s scan rate. If only a small amount of water is added (10 to 40 μL total) the corrosion is no longer apparent (Figure 6(ii)). The PL_{fb} value stays constant and the cell appears to be passivated from corrosion. We attribute this to the formation of a thin oxide layer that charge can still transfer through (hence no change in the $I-V$ behavior) but that is preventing the buildup of photoinduced SS. When 60$-$100 μL of water is added, the cell again shows corrosion (Figure 6(iii)). With each water addition in this range, the cell takes less time to corrode and has a larger drop in PL_{fb}. When enough water is added, it appears to overcome the thin protective layer and once again causes the cell to corrode. Once >110 μL of water is added to the cell, the Fermi level becomes pinned by the growing density of SS from the oxide buildup, the PL loses its voltage dependence, and the PL$-V$ curve becomes a flat line (not shown in Figure 6). At this point, the corrosion of the cell can no longer be monitored.

We conclude that the impact of water on these cells is concentration dependent. The trace amounts of water in the "dry", or fresh, cell allow corrosion to occur. A small amount of water added to the cell coats the semiconductor with oxide and protects it from further corrosion. Once the 40 μL threshold is passed, however, further water additions cause the cell to photocorrode more rapidly. If >110 μL of water is added, the oxide buildup pins the Fermi level of the semiconductor and the voltage dependence to the PL is lost entirely.

IV. Conclusions

There is a significant amount of information to be learned from the asymmetry of the PL$-V$ scans. Both the dip in the PL as the voltage is scanned and the difference in PL$-V$ profile with scan direction are unexpected from the solid-state view of the interface where the band bending dominates the PL characteristics. Clearly, in these cells, electrochemistry has a significant impact on the photoluminescence, even 0.6 V from the flat band potential. The differences in PL$-V$ behavior from the predictions of the MDLM are attributed to the cathodic current from the majority carrier reducing ferricenium at the interface. The trend of TRPL decay rates with applied potential follows the trend of the PL$-V$ scans.

The applied potential dramatically affects the condition of the interface and the PL produced by the picosecond light pulses as seen by the PL$-T$ scans in Figure 3. Near V_{fb}, the cell photowashes, decreasing the density of SS and increasing the amount of PL produced. In deep depletion (0.0 V) the cell corrodes, increasing the density of SS and decreasing the measured PL. Cell corrosion can be seen in the PL$-V$ scans by an overall decrease in PL, by the loss of the PL dip at -1.0 V, and by splitting of the PL peak around V_{fb}.

Other cell parameters also affect the rate of corrosion of the GaAs. The presence of the redox couple has a dramatic effect on cell corrosion. The cell corrodes much faster in a cell with no redox couple to compete for the available holes. Also, the concentration of water in the cell has an effect on cell corrosion. Water additions can either passivate the cell or cause the cell to corrode faster. However, once enough water is added, the Fermi level of the GaAs becomes pinned and the PL$-V$ scans become flat lines, providing no additional information about the interface.

We hope this information will be useful to others who wish to make use of these nonaqueous photoelectrochemical cells. A great deal of control can be had over the characteristics and behavior of these cells by controlling the redox couple, the applied potential, and the water content. However, this also implies that great care must also be taken to stabilize the environment that these cells are kept in if one is to perform meaningful investigations on them.

Acknowledgment. We gratefully acknowledge the financial support of the Department of Energy, Basic Energy Sciences (Grant DE-FG06-86ER45273).

References and Notes

(1) Allongue, P.; Blonkowski, S. *J. Electroanal. Chem.* **1991**, *316*, 57$-$77.

(2) Allongue, P.; Blonkowski, S. *J. Electroanal. Chem.* **1991**, *317*, 77$-$99.

(3) Balko, B. A.; Richmond, G. L. *J. Phys. Chem.* **1993**, *97*, 9002$-$9008.

(4) Balko, B. A.; Miller, E. A.; Richmond, G. L. *J. Phys. Chem.* **1995**, *99*, 4124$-$4131.

(5) Bard, A. J.; Wrighton, M. S. *J. Electrochem. Soc.* **1977**, *124*, 1706$-$1710.

(6) Jr., K. W. F.; Madou, M. J.; Morrison, S. R. *J. Phys. Chem.* **1980**, *84*, 3172−3178.
(7) Jr., K. W. F.; Madou, M. J.; Morrison, S. R. *J. Electrochem. Soc.* **1981**, *128*, 1527−1531.
(8) Lingier, S.; Vanmaekelbergh, D.; Gomes, W. P. *J. Electroanal. Chem.* **1987**, *228*, 77−88.
(9) Schroder, K.; Memming, R. *Ber. Bunsen-Ges. Phys. Chem.* **1985**, *89*, 385−392.
(10) Vanmaekelbergh, D.; Gomes, W. P. *J. Phys. Chem.* **1990**, *94*, 1571−1575.
(11) Gerischer, V. H. *Ber. Bunsen-Ges. Phys. Chem.* **1965**, *69*, 578−583.
(12) Gerischer, H. *J. Electroanal. Chem.* **1977**, *82*, 133−143.
(13) Bessolov, V. N.; Lebedev, M. V.; Binh, N. M.; Friedrich, M.; Zahn, D. R. T. *Semicond. Sci. Technol.* **1998**, *13*, 611−614.
(14) Ellis, A. B.; Bolts, J. M.; Kaiser, S. W.; Wrighton, M. S. *J. Am. Chem. Soc.* **1977**, *99*.
(15) Ohno, T. *Phys. Rev. B.* **1991**, *44*, 6306−6311.
(16) Sandroff, C. J.; Nottenburg, R. N.; Bischoff, J.-C.; Bhat, R. *Appl. Phys. Lett.* **1987**, *51*, 33−35.
(17) Sandroff, C. J.; Hegde, M. S.; Farrow, L. A.; Chang, C. C.; Harbison, J. P. *Appl. Phys. Lett.* **1989**, *54*, 362−364.
(18) Sugiyama, M.; Maeyama, S.; Oshima, M. *Phys. Rev. B* **1993**, *48*, 11037−11042.
(19) Yablonovitch, E.; Sandroff, C. J.; Bhat, R.; Gmitter, T. *Appl. Phys. Lett.* **1987**, *51*, 439−441.
(20) Yamada, C.; Kimura, T.; Fuqua, P. *Jpn. J. Appl. Phys.* **1992**, *31*, L1657−L1660.
(21) Lunt, S. R.; Ryba, G. N.; Santangelo, P. G.; Lewis, N. S. *J. Appl. Phys.* **1991**, *70*, 7449−7467.
(22) Yan, Y. *Appl. Phys. Lett.* **1997**, *71*, 407−409.
(23) Lewis, N. S. *J. Phys. Chem. B* **1998**, *102*, 4843−4855.
(24) Lingier, S.; Gomes, W. P.; Cardon, F. *Ber. Bunsen-Ges. Phys. Chem.* **1989**, *93*, 2−7.
(25) Smith, B. B.; Nozik, A. J. *J. Phys. Chem. B* **1997**, *101*, 2459−2475.
(26) Oigawa, H.; Fan, J.-F.; Nannichi, Y. *Jpn. J. Appl. Phys.* **1989**, *28*, L525−L527.
(27) Ives, N. A.; Stupian, G. W.; Leung, M. S. *Appl. Phys. Lett.* **1987**, *50*, 256−258.
(28) Ives, N. A.; Stupian, G. W.; Leung, M. S. *Appl. Phys. Lett.* **1990**, *56*, 1537−1539.
(29) Kauffman, J. F.; Richmond, G. L. *Appl. Phys. Lett.* **1991**, *59*, 561−563.
(30) Bard, A. J.; Bocarsly, A. B.; Fan, F.-R. F.; Walton, E. G.; Wrighton, M. S. *J. Am. Chem. Soc.* **1980**, *102*, 3671−3677.
(31) Morrison, S. R. *Electrochemistry at Semiconductor and Oxidized Metal Electrodes*; Plenum Press: New York, 1980.
(32) Pleskov, Y. V.; Gurevich, Y. Y. *Semiconductor Photoelectrochemistry*; Consultants Bureau: New York, 1986.
(33) Ba, B.; Fotouhi, B.; Gabouze, N.; Gorochov, O.; Cachet, H. *J. Electroanal. Chem.* **1992**, *334*, 263−277.
(34) Abshere, T. A.; Richmond, G. L. *J. Phys. Chem. B* **1999**, *103*, 7911−7919.
(35) Miller, E. A.; Richmond, G. L. *J. Phys. Chem. B* **1997**, *101*, 2669−2677.
(36) Kauffman, J. F.; Balko, B. A.; Richmond, G. L. *J. Phys. Chem.* **1992**, *96*, 6374−6377.
(37) Kauffman, J. F.; Richmond, G. L. *J. Appl. Phys.* **1993**, *73*, 1912−1917.
(38) Smandek, B.; Chmiel, G.; Gerischer, H. *Ber. Bunsen-Ges. Phys. Chem.* **1989**, *93*, 1094−1103.
(39) Kauffman, J. F.; Balko, B. A.; Richmond, G. L. *J. Phys. Chem.* **1992**, *96*, 6371−6374.
(40) O'Connor, D. V.; Phillips, D. *Time-Correlated Single Photon Counting*; Academic Press: London, 1984.
(41) Yariv, A. *Optical Electronics*; Holt, Rinehart, & Winston: New York, 1986.
(42) Janietz, P.; Weiche, R.; Westfahl, J.; Landsberg, R. *J. Electroanal. Chem.* **1980**, *112*, 63−70.
(43) Kohl, P. A.; Bard, A. J. *J. Electrochem. Soc.* **1979**, *126*, 603−608.
(44) Ando, K.; Yamamoto, A.; Yamaguchi, M. *J. Appl. Phys.* **1980**, *51*, 6432−6434.
(45) Chmiel, G.; Gerischer, H. *J. Phys. Chem.* **1990**, *94*, 1612−1619.
(46) Hobson, W. S.; Ellis, A. B. *J. Appl. Phys.* **1983**, *54*, 5956−5960.
(47) Langmann, U. *Appl. Phys.* **1973**, *1*, 219−221.